

Evaluation of Longitudinal Desired Dynamics for Dynamic-Inversion Controlled Generic Reentry Vehicles

Jennifer Georgie and John Valasek

Texas A&M University, College Station, Texas 77843-3141

Dynamic inversion is a control synthesis technique in which the inherent dynamics of a dynamical system are canceled out and replaced by desired dynamics, selected by the designer. The output of such an inner-loop controller is the control input, which produces the desired closed-loop response. The desired dynamics essentially form a loop-shaping compensator that affects the closed-loop response of the entire system. This paper attempts to quantify the effect of different forms of desired dynamics on the closed-loop performance and robustness of a dynamic-inversion flight controller for reentry vehicles. Proportional, proportional-integral, flying-quality, and ride-quality forms of desired dynamics are evaluated using time-domain specifications, robustness requirements on singular values, quadratic cost, and a passenger ride comfort index. Longitudinal controllers are synthesized for a generic X-38 type crew return vehicle, using a set of linear models at subsonic, transonic, and hypersonic flight conditions. For the candidate forms of desired dynamics and inversion controller structures evaluated here, results indicate that the form used impacts closed-loop performance and robustness and more so for some inversion controller structures more than others. The ride-quality dynamics used with a two-loop angle-of-attack inversion controller provide the best overall system performance, in terms of both time-domain and frequency-domain specifications, and the evaluation criteria.

Introduction

RENTRY vehicles must operate over a broad flight envelope, spanning hypersonic flight to subsonic flight to landing. The aerodynamic characteristics within this envelope vary widely. A controller based on classical control methodologies,^{1,2} such as root locus design, would require synthesis of many different designs at selected operating points along the flight path. These classical methodologies can be time consuming, thereby increasing both design time and cost during control system development. Additionally, gains need to be scheduled across the flight envelope. In contrast, dynamic inversion is a candidate methodology that seeks to eliminate

gain scheduling through the inversion and cancellation of the inherent dynamics, by replacement with a set of user-selected desired dynamics. The need to gain schedule is thus reduced through the use of a high-fidelity, onboard aircraft model. For these reasons dynamic inversion is a promising candidate control design methodology aircraft with extensive flight envelopes, like reentry vehicles.

Within the last decade dynamic inversion has become a popular methodology for aircraft flight controller design. Much of the literature has applied this design methodology to both the longitudinal and lateral/directional axes of high-performance aircraft, such as the F-117A,³ the F-18 HARV,⁴ and other modified versions of the F-18⁵



Jennifer Georgie of Victoria, Texas, earned the B.S. and M.S. degrees in aerospace engineering from Texas A&M University in 1999 and 2001, respectively. She is a recipient of the Distinguished Student Award for Outstanding Academic Achievement from the College of Engineering. From 1996 to 1998 she served three co-op tours at the NASA Dryden Flight Research Center, working in the X-31 Flight Controls Group and on the Russian High Speed Civil Transport program in the Aerodynamics Group. For her efforts she was awarded the NASA Dryden Stephen B. Davis Outstanding Co-Op Award and the NASA Dryden Spotlight Award twice. From 1999 to 2001 she was a graduate research assistant at Texas A&M, where she worked on flight testing a vision-based automatic landing system and on dynamic inversion controllers for reentry vehicles as a graduate summer intern with the NASA Johnson Space Center. Since June 2001, she has been with Lockheed Martin Aeronautics Company, Fort Worth, Texas, where she is a flight control engineer in the F-16 Block 60 Control Law Design and Analysis group. She is a Member of AIAA.



John Valasek earned the B.S. degree in aerospace engineering from California State Polytechnic University, Pomona, in 1986 and the M.S. degree with honors and the Ph.D. in aerospace engineering from the University of Kansas in 1991 and 1995, respectively. He was a flight control engineer for the Northrop Corporation, Aircraft Division, from 1985 to 1988, where he worked in the Flight Controls Research Group and on the AGM-137 Tri-Service Standoff Attack Missile (TSSAM) program. From 1995 to 1997 he was on the faculty of the mechanical and aeronautical engineering department at Western Michigan University and in 1997 was an Air Force Office of Scientific Research Summer Faculty Research Fellow for the Flight Dynamics Directorate at the Air Force Research Laboratory, Dayton, Ohio. Since then, he has been with Texas A&M University, where he is an associate professor of aerospace engineering and director of the Flight Simulation Laboratory. He teaches courses on digital flight control, nonlinear systems, flight mechanics, and aircraft design. Current research interests include intelligent autonomous vehicle control, vision-based navigation systems, fault-tolerant adaptive control, and air traffic management systems. He is an Associate Fellow of AIAA and current Chairman of the AIAA Atmospheric Flight Mechanics Technical Committee.

Received 2 April 2001; presented as Paper 2001-4382 at the AIAA Guidance, Navigation, and Control Conference, Montreal, Canada, 6–9 August 2001; revision received 13 February 2003; accepted for publication 13 May 2003. Copyright © 2003 by Jennifer Georgie and John Valasek. Published by the American Institute of Aeronautics and Astronautics, Inc., with permission. Copies of this paper may be made for personal or internal use, on condition that the copier pay the \$10.00 per-copy fee to the Copyright Clearance Center, Inc., 222 Rosewood Drive, Danvers, MA 01923; include the code 0731-5090/03 \$10.00 in correspondence with the CCC.

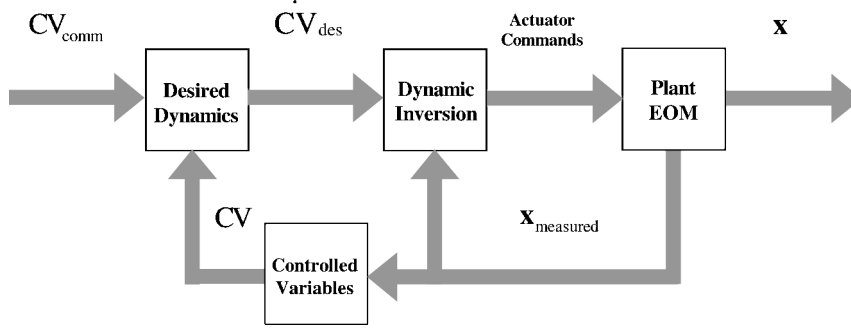


Fig. 1 Dynamic inversion.

and the F-16.⁶ Dynamic inversion is similar to model-following control, in that both methodologies invert dynamical equations of the plant.⁷ Whereas model-following control specifies the desired plant behavior with an internal model to be followed, dynamic inversion specifies the desired plant behavior explicitly by specifying the rate of the desired state, or of the controlled variable (CV), a weighted function of the desired states, and not the state itself. A block diagram representation of the general dynamic inversion process is shown in Fig. 1. The output of the dynamic-inversion block is the control input required to achieve the desired vehicle response.

For the case of perfect cancellation, the desired dynamics are exactly the new dynamics of the system. However, most practical applications contain uncertainties that prevent a perfect cancellation of the inherent dynamics. Additionally, because different types of desired dynamics will respond differently to uncertainties it is important that the desired dynamics be robust. Three different forms of desired dynamics have seen use in aircraft applications. Representative examples include a proportional form used by Smith and Berry for a Harrier⁸; a proportional plus integral form used by Colgren and Enns for an F-117A,³ Enns et al. for the F-18 HARV,⁴ and Adams and Banda for an F-16⁶; and a form based upon flying qualities used by Ostroff and Bacon for a generic high-performance fighter⁹ and Brinker and Wise for a prototype aircraft.¹⁰ Rationale for selecting the form of desired dynamics are discussed briefly in Ref. 11, and Fer and Enns detail an approach in Ref. 12 for selecting gains for the proportional form of desired dynamics. A fourth-candidate form of desired dynamics is a form based on desired passenger-ride-quality dynamics.

This paper investigates the following forms of candidate desired dynamics: 1) proportional dynamics, 2) proportional plus integral dynamics, 3) dynamics satisfying a desired level of flying quality, and 4) dynamics corresponding to passenger ride quality. It evaluates them in terms of performance, robustness, a quadratic cost, and a passenger-ride comfort index. The basic form of a dynamic inversion control law is developed, and the extension to a two-timescale approach is briefly discussed. The dynamic-inversion methodology and the desired dynamics investigation are illustrated with a longitudinal design example based on linear models of a generic X-38 type reentry vehicle. Closed-loop system performance is evaluated in terms of time-domain performance specifications and in terms of singular values in the frequency domain. The responses of each set of desired dynamics are compared to each other in terms of the design specifications, a user-specified quadratic cost function, and a passenger-ride-quality comfort rating index.

Dynamic Inversion

Dynamic inversion is a control design methodology that uses a feedback signal to cancel inherent dynamics and simultaneously achieve a specified desired dynamic response.¹³ Consider a general time-invariant nonlinear system modeled by the ordinary differential equations

$$\dot{x} = f(x) + g(x, u) \quad (1)$$

$$y(t) = H(x, u) \quad (2)$$

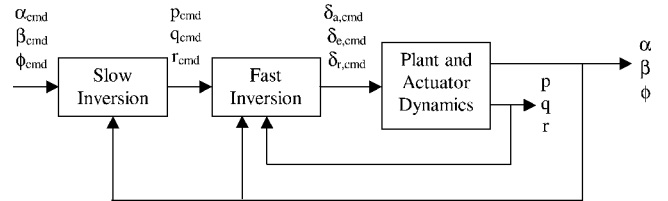


Fig. 2 Two-timescale inversion of slow dynamics.

with state vector $x \in \mathbb{R}^n$ and control vector $u \in \mathbb{R}^m$ and n is the number of states and m is the number of controls. If the system is affine in the controls, then solving explicitly for the control vector yields

$$u = g(x)^{-1}[\dot{x} - f(x)] \quad (3)$$

The only requirement for Eq. (3) to be an admissible control law is that $g(x)^{-1}$ must exist for all admissible values of x . Because $g(x)$ is generally not full rank for differentially nonflat systems, that is, systems in which there are more states than control inputs, the number of states that can be inverted must be less than or equal to the number of control inputs available. This can often be overcome by combining several states into the controlled variable or using a pseudoinverse. Replacement of the inherent dynamics with the desired dynamics results in the control that will produce the desired dynamics:

$$u = g(x)^{-1}[\dot{x}_{des} - f(x)] \quad (4)$$

For example, if it is desired to control the short period mode of an aircraft, angle of attack α and body-axis pitch rate q are selected as the controlled states. If desired, normal load factor can be used in place of angle-of-attack. For the pitch-rate controlled state inverting the pitch acceleration dynamics leads to the form of Eq. (4), which yields a control law for the required elevon deflection $\delta_{e,cmd}$:

$$\delta_{e,cmd} = (M_{\delta_e})^{-1}[\dot{q}_{des} - M_{\alpha}\alpha - M_q q] \quad (5)$$

where M_{α} , M_q , M_{δ_e} are the dimensional pitching-moment derivatives caused by perturbations in angle of attack, pitch rate, and elevon deflection, respectively. Provided M_{δ_e} is invertible, this control law implies that $\dot{q} \equiv \dot{q}_{des}$ so that the system now has the desired pitch-rate dynamics.

Even if $g(x)$ is of full rank, problems can arise if its magnitude is small because inversion can produce large control inputs. A two-timescale method has been developed and applied in previous research to work around such a problem.^{10,14} In this method the control surface is used to generate the pitch-rate dynamics \dot{q} directly. The resulting pitch rate is then used to control $\dot{\alpha}$. Figure 2 illustrates this approach in which two dynamic-inversion loops are present: a fast inner-loop inversion for commanding rotational-rate variables, such as q , and a slow outer-loop inversion for commanding rotational variables, such as α . The multiple timescale method seeks to reformulate the original differential equation of Eq. (1) into a set of

two separate differential equations: a set of slow dynamics \dot{x} and a set of fast dynamics \dot{y} :

$$\dot{x} = f(x) + g(x)y \quad (6)$$

$$\dot{y} = h(x, y) + k(x, y)u \quad (7)$$

Substituting for the linear aircraft dynamics represented as $\dot{x} = Ax + Bu$ yields a set of slow dynamic equations for the rotational variables and a set of fast dynamic equations for the rotational-rate variables. The rate variables now form the input for the slow dynamics, while the actual control surface commands form the inputs for the rate dynamics. Inverting the slow and fast differential equations yields the two dynamic-inversion control laws for the outer dynamic inversion loop and inner dynamic inversion loop, whose block diagram is shown in Fig. 2. A full and detailed derivation of these equations is contained in Ref. 15. Several observations can be made from these dynamic-inversion control law equations. Only the short-period aerodynamic terms are present in both sets of slow and fast dynamics, and the control effectiveness of the elevator in influencing angle of attack Z_{δ_e}/U_0 is not present in the inversion matrix and has been eliminated altogether from these two sets of equations. Therefore, only the control input matrix terms for the rate dynamics have been kept. This is beneficial because the control surfaces typically are more effective on the rate variables than on the position variables.

In theory, if the modeling of the plant dynamics is perfect an exact cancellation is achieved. However, in practice the system plant cannot be modeled exactly, thereby preventing an exact replacement of the inherent plant dynamics with the desired dynamics. Consequently, the cancellation caused by dynamic inversion introduces errors or uncertainties into the system, such as unmodeled actuator and sensor dynamics, and/or errors in both of these components. Good disturbance rejection and low sensitivity are desirable features of all controllers, which dynamic inversion alone might not guarantee. If needed, a robust outer-loop controller can be synthesized around the dynamic-inversion inner loop to achieve desired levels of robustness.¹⁶ A pole-placement feedback compensator was selected for the examples in this paper because it is straightforward to use and possesses desirable stability and robustness properties.

Desired Dynamics

Different forms of desired dynamics will respond differently when subjected to the same uncertainties. It is therefore important to select the form of desired dynamics that will satisfy specified performance and robustness requirements. An important consideration in selecting these dynamics is that they must be achievable, given the limitations of the vehicle's effectors.⁹ If the desired dynamics require the system to generate more forces and moments than the effectors are capable of producing, then the effectors might saturate. The final closed-loop response is found according to the block diagram shown in Fig. 3. The integrator to the right of the desired dynamics is used to approximate the rest of the system dynamics, which includes such elements as actuator dynamics, dynamic inversion, airplane dynamics, and sensors.¹¹

The proportional form of desired dynamics for a given CV is

$$\dot{C}V_{des} = K_{\omega}(CV_{cmd} - CV) \quad (8)$$

The constant K_{ω} amplifies the error between the CV command and its feedback term. A block diagram representation of the proportional dynamic is shown in Fig. 4a. The closed-loop transfer function

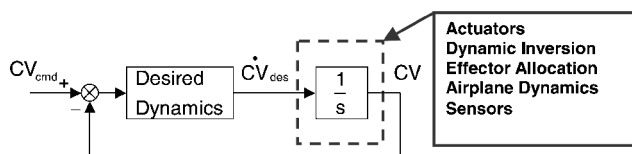


Fig. 3 Block diagram corresponding to closed-loop transfer function.

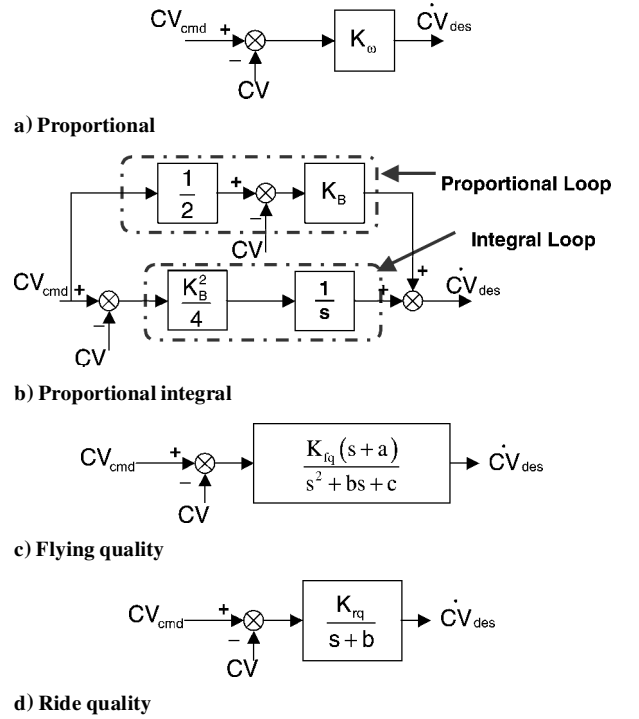


Fig. 4 Forms of desired dynamics.

shown in Eq. (9) places a single pole at $s = -K_{\omega}$:

$$CV/CV_{cmd} = K_{\omega}/s + K_{\omega} \quad (9)$$

The proportional-integral (PI) form of desired dynamics has the form

$$\dot{C}V_{des} = K_B \left(\frac{1}{2} CV_{cmd} - CV \right) + \left(\frac{K_B^2}{4s} \right) (CV_{cmd} - CV) \quad (10)$$

with closed-loop transfer function

$$CV/CV_{cmd} = \frac{1}{2} K_B / s + \frac{1}{2} K_B \quad (11)$$

which places a pole at $s = -0.5K_B$ for any real constant K_B . In essence, it compensates for both the CV and the CV rate. The block-diagram representation for the proportional plus integral dynamics is shown in Fig. 4b.

For aircraft applications desired dynamics can also be specified in terms of flying-quality levels. Reference 17 contains flying-quality specifications according to vehicle class and mission type, from which proper time-domain characteristics (frequency, damping ratio, time constant) corresponding to a desired flying-quality level can be selected. These characteristics can be translated directly into values for gains and pole locations. The flying-quality desired dynamics, shown in Fig. 4c, can be represented as

$$\dot{C}V_{des} = \frac{K_{fq}(s+a)}{s^2 + bs + c} (CV_{cmd} - CV) \quad (12)$$

where $b = 2\zeta_{des}\omega_{n,des}$ and $c = \omega_{n,des}^2 - K_{fq}$ for the desired damping, ζ_{des} , and natural frequency $\omega_{n,des}$. Both the gain K_{fq} and zero location a are real constant values. The closed-loop transfer function for the flying-quality dynamics is given by

$$\frac{CV}{CV_{cmd}} = \frac{K_{fq}(s+a)}{s^3 + bs^2 + (c + K_{fq})s + K_{fq}a} \quad (13)$$

These dynamics place three closed-loop poles and add a zero to the system.

The ride-quality desired dynamics, shown in Fig. 4d, are given by

$$\dot{C}V_{des} = K_{rq}/(s+b)(CV_{cmd} - CV) \quad (14)$$

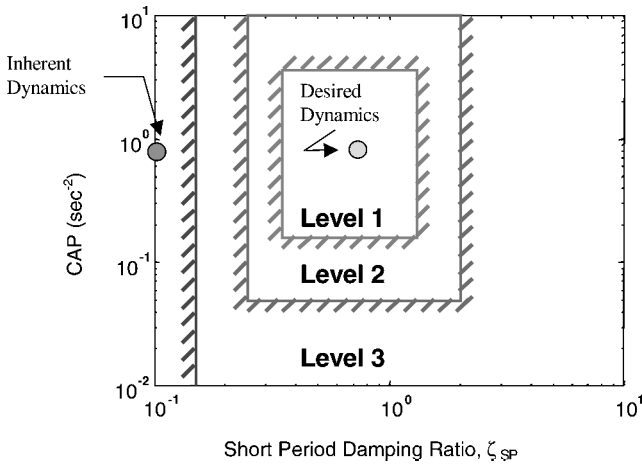


Fig. 5 CAP requirements.

The closed-loop transfer function for the ride quality is

$$\frac{CV}{CV_{cmd}} = \frac{K_{rq}}{s^2 + bs + K_{rq}} \tag{15}$$

which places two closed-loop poles at $s_{1,2} = -0.5b \pm 0.5\sqrt{(b^2 - 4K_{rq})}i$ for real constants b and K_{rq} . For highly augmented aircraft Ref. 17 recommends use of the control anticipation parameter (CAP), Eq. (16), in place of specifications on the short period mode:

$$CAP = \omega_n^2 / n_\alpha \tag{16}$$

The ride-quality dynamics are designed by first selecting a value of damping ratio and a value of CAP that lie within the level I box in Fig. 5. With this CAP value and a value for gust induced load factor n_α ,

$$n_\alpha = \frac{\partial n}{\partial \alpha} = \frac{C_{L\alpha} \bar{q}}{(W/S)} \tag{17}$$

where the numerator is the product of airplane lift-curve slope and dynamic pressure and the denominator is the wing loading of the aircraft. Equation (16) is then used to solve for the corresponding value of frequency. With the frequency and damping ratio now specified, the gain and pole locations can be determined.

Pole Placement

An eigenstructure-assignment, or pole-placement, method can be used to find the gains required to achieve a specified set of closed-loop eigenvalues, or poles. It is essentially an inverse eigenvalue problem,¹⁸ and because of its simple gain feedback compensation this technique will not mask the effect of the desired dynamics on the dynamic-inversion controllers presented here. For multivariable control systems pole assignment by state feedback is generally an underdetermined problem, in that for controllable systems an infinity of gain matrices exist for a given set of eigenvalue locations.¹⁹

For a linear time-invariant system $\dot{x} = Ax + Bu$, the following state-feedback control is used to modify the eigenvalues of the system:

$$u = -Gx \tag{18}$$

where G is the feedback gain matrix. In the pole-placement method the following assumptions are made: full-state feedback, the pair (A, B) is controllable, and B is of full rank. Provided these assumptions hold, the closed-loop system dynamics are now

$$\dot{x} = (A - BG)x \tag{19}$$

Equations (20) and (21) show the corresponding eigenvalue problems¹⁹

$$(A - BG)\varphi_i = \lambda_i \varphi_i \tag{20}$$

$$(A - BG)^T \psi_i = \lambda_i \psi_i \tag{21}$$

where φ_i and ψ_i are the right and left eigenvectors respectively, corresponding to the eigenvalue λ_i . The eigenvectors are then scaled according to $\varphi_i^* \varphi_i = 1$ and $\psi_i^T \varphi_j = \delta_{ij}$, where $*$ is the conjugate transpose. The parameter vector $h_i \in \mathbb{R}^m$ is now introduced and defined in Eq. (22):

$$h_i = G\varphi_i \tag{22}$$

The eigenvalue problems can then be rewritten as a generalized Lyapunov equation known as Sylvester's equation:

$$A\Phi - \Phi\Lambda = B H \tag{23}$$

where $\Phi = [\varphi_1, \varphi_2, \dots, \varphi_n]$, $\Lambda = \text{diag}[\lambda_1, \lambda_2, \dots, \lambda_n]$, and $H = [h_1, h_2, \dots, h_n]$. For a given pair (A, B) and for a prescribed Λ , a parameter matrix H can be chosen, from which Eq. (23) can be used to solve for Φ . Then, the gain matrix G is then found according to

$$G\Phi = H \tag{24}$$

The feedback matrix G is obtained by assigning linearly independent eigenvectors, corresponding to the required eigenvalues, such that the matrix of eigenvectors is as well conditioned as possible.¹⁸ Many approaches exist to finding such well-conditioned eigenvectors, and each method differs in the selection of criteria that determines the closed-loop eigenvectors. It is also desirable for the closed-loop eigenvectors to be orthogonal in order to minimize the sensitivity of the eigenvalue placement to model errors. The assigned poles are then as insensitive to perturbations in the system and gain matrices as possible, and the resulting feedback matrix is as reasonably bounded as can be expected. In addition, the lower bound on the stability margin is maximized.¹⁸ In cases where well-conditioned solutions are expected, near optimal results are obtained.

Generic Reentry Vehicle Model

The set of candidate desired dynamics is evaluated using linear models of a generic reentry vehicle based on the X-38 (Fig. 6). The configuration has two sets of control surfaces: a pair of elevon control surfaces for pitch and roll control and a pair of rudders for yaw control (Fig. 7). The actuators for each control effector



Fig. 6 X-38 Flight Demonstrator.

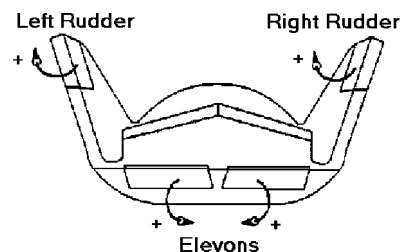


Fig. 7 X-38 control surfaces with positive sign convention.

Table 1 Desired dynamics selection

Desired dynamics	Pitch-rate case	Angle-of-attack case	
		Slow inversion	Fast inversion
Proportional	0.4 rad/s	0.8 rad/s	1.3 rad/s
Proportional integral	$5\left(\frac{1}{2}CV_{cmd} - CV\right) + \frac{6.25}{s}(CV_{cmd} - CV)$	$\left(\frac{1}{2}CV_{cmd} - CV\right) + \frac{2}{s}(CV_{cmd} - CV)$	$6\left(\frac{1}{2}CV_{cmd} - CV\right) + \frac{6.25}{s}(CV_{cmd} - CV)$
Flying quality	$\frac{1.2(s+0.8)}{s^2+2.24s+1.96}$	$\frac{1.4(s+0.8)}{s^2+2.24s+1.96}$	$\frac{1.5(s+0.8)}{s^2+2.24s+1.96}$
Ride quality	$\frac{1.96}{s+2.24}$	$\frac{1.96}{s+3}$	$\frac{7}{s+4}$

are modeled as second-order transfer functions with damping ratio 0.707 and natural frequency 26 rad/s. The position and rate limits of the longitudinal control surfaces are²⁰

$$0 \text{ deg} \leq \delta_e \leq 45 \text{ deg}$$

$$-50 \text{ deg/s} \leq \dot{\delta}_e \leq 50 \text{ deg/s}$$

Starting with the four-state parametric longitudinal linear model shown in the Appendix, it is desired to control the short-period mode using angle of attack and pitch rate. Applying the short-period approximation, only the terms in the model corresponding to angle of attack and pitch rate are retained, and the standard assumption of $M_{\dot{\alpha}}$ and Z_{δ_e} equal to zero is also applied. These assumptions result in the linearized equations of motion for pitch acceleration and angle-of-attack rate, respectively:

$$\dot{q} = M_{\alpha}\alpha + M_q q + M_{\delta_e}\delta_e \quad (25)$$

$$\dot{\alpha} = (Z_{\alpha}/u_o)\alpha + (1 + Z_q/u_o)q + (Z_{\delta_e}/u_o)\delta_e \quad (26)$$

In this model sensor dynamics are neglected, and the measurement error in the feedback states α and q are assumed to be zero. The short-period mode cannot be completely replaced because there is only one longitudinal control effector, and thus only one longitudinal state can be directly inverted. To proceed, a single fast dynamic-inversion loop is used for inverting the pitch-rate dynamics, and a two-timescale approach is applied in the inversion of angle-of-attack dynamics. The elevon input that cancels the inherent pitch-rate dynamics and produces the desired pitch-rate response is shown in Eq. (27). Because a two-timescale approach is used to invert the angle-of-attack dynamics, two dynamic-inversion control laws must be implemented, each requiring a set of desired dynamics. Equation (28) shows the pitch-rate command generated by the slow outer-loop inversion, and Eq. (27) shows the elevon command, generated by the fast inner loop, required to produce a desired angle-of-attack response. Both control laws require both angle-of-attack and pitch-rate feedback, which is full-state feedback for the short-period approximation:

$$\delta_{e,cmd} = (M_{\delta_e})^{-1}(\dot{q}_{des} - M_{\alpha}\alpha - M_q q) \quad (27)$$

$$q_{cmd} = (1 + Z_q/U_o)^{-1}[(\dot{\alpha}_{des} - (Z_{\alpha}/U_o)\alpha] \quad (28)$$

The form of the desired dynamics selected for the controlled variable, pitch rate in Eq. (27), and angle of attack in Eq. (28) is left to the designer. The numerical examples that follow use the candidate forms of desired dynamics discussed earlier for the controlled variable.

Numerical Examples

Method and Scope

The four different forms of desired dynamics discussed in the paper are analyzed for two types of inversion test cases: a pitch-rate case using Eq. (27) and an angle-of-attack case using Eq. (28), both corresponding to a transonic flight condition. Gains are tuned as needed to simultaneously satisfy both the time- and frequency-domain requirements presented in the next section. The most

promising form of desired dynamics from each test case is then evaluated anew for a range of Mach numbers corresponding to the subsonic, transonic, and hypersonic flight conditions shown in the Appendix. Although the hypersonic flight condition is on the low-hypersonic/high-supersonic range, it is representative of higher Mach numbers because the model parameters change little up to the higher Mach numbers, where the vehicle is still in completely aerodynamically controlled flight. Table 1 summarizes the desired dynamics forms selected for the pitch-rate cases and the angle-of-attack cases. Each set of dynamics acts on the error between the CV command and its feedback term. The proportional, PI, and flying-qualities desired dynamics are selected to satisfy the frequency and damping ratio specifications presented in the next section, whereas the ride-qualities dynamics are selected as already described, using the CAP value and damping ratio shown in Fig. 5. For the two-timescale approach in the angle-of-attack cases, the fast inner loop was designed using the responses from initial condition inputs on pitch rate. The outer loop was then designed using pole placement to generate gains for the feedback path. All simulations are performed in MATLAB's[®] Simulink environment, using a parametric full-state longitudinal state-space linear model, for the subsonic, transonic, and hypersonic flight conditions shown in the Appendix.

Besides the specifications introduced in the next section, two numeric indices are used as quantitative aids for evaluating performance. The quadratic cost function of Eq. (29) is used to generate a scalar value, or cost, of the performance of each controller in terms of the four longitudinal states and the elevon control:

$$J = \mathbf{x}^T Q \mathbf{x} + \mathbf{u}^T R \mathbf{u} \quad (29)$$

The weighting matrices Q and R are selected by the designer, according to the objective of the test case. Because the phugoid mode is of little importance here, the velocity and pitch attitude states are weighted less than the short-period states. For the pitch-rate cases it is desired to weight pitch rate more heavily than angle of attack and vice versa for the angle-of-attack cases. Thus state weights $Q = \text{diag}(0.1 \ 1 \ 10 \ 0.1)$ are used for the pitch-rate cases, and $Q = \text{diag}(0.1 \ 10 \ 1 \ 0.1)$ for the angle-of-attack cases; the control weight is set to $R = 1$ for both cases. The second numeric index is a passenger-ride comfort index from Richards et al., whose numerical value cross indexed on an associated linear scale of 1 (very comfortable) to 4 (acceptable; neutral) to 7 (very uncomfortable) quantifies not only passengers' perception of the smoothness or roughness of the ride, but also the ride levels that produce motion sickness.²¹ This is an important consideration because passengers on reentry vehicles might be injured, ill, or incapacitated, which mandates that the ride be smooth and the passengers stressed as little as possible. The comfort index is empirically based upon extensive research with human subjects and has been shown an accurate indicator of passenger perceptions of ride quality and motion sickness in air vehicles²²:

$$C = 2.1 + 17.2\bar{a}_z \quad (30)$$

The comfort index C is dimensionless, and the rms vertical acceleration in units of g , \bar{a}_z is defined as $\bar{a}_z = (1/g)[U_1\dot{\alpha} - U_1 \cos(\alpha_1)q + g \sin(\theta_1)\theta]$, with subscripts denoting trim values.

Vertical accelerations are induced by both maneuvers and turbulence, and the rms value was calculated over the duration of the simulation run. Lower values of the comfort index indicate greater passenger ride comfort and less susceptibility to motion sickness.

Specifications

Each test case is designed according to time-domain performance specifications and frequency-domain robustness specifications. The desired short-period frequency and damping ratio are selected from Mil-STD-1797A¹⁷ to satisfy level I flying qualities for a class II vehicle during a category C flight phase:

$$0.35 \leq \zeta \leq 1.30$$

$$0.6 \text{ rad/s} \leq \omega_n \leq 1.4 \text{ rad/s}$$

The test input is a unit step, with rise time, settling time, and overshoot specified by the envelope in Fig. 8, which correspond to level I flying qualities for this vehicle. The elevator position and rate limits must remain within the bounds indicated earlier.

The robustness analysis is adapted from Ito and Valasek in Ref. 23, using a sigma-Bode plot of the loop gain maximum and minimum singular values over a range of input frequencies. The stability robustness and performance robustness specifications are 1) zero steady-state error, 2) attenuation of low-frequency disturbances by a factor of 0.1, 3) linear model accurate to within 10% of actual plant for frequencies up to 2 rad/s and grows without bound at 20 dB/decade thereafter, and 4) attenuate motions in the motion sickness frequency range of 0.6 to 1.6 rad/s to alleviate passenger discomfort.²⁴ Reference 23 shows how to translate these requirements into boundaries on the magnitudes of the singular values at certain frequencies. For compliance, the singular values must lie between the performance boundary and stability boundary over all frequencies of interest.

Results

Results for the closed-loop inverted pitch dynamics test case are presented in Figs. 9 and 10 and Tables 2 and 3. Figure 9 shows the state and control responses for each form of desired dynamics to be smooth, well behaved, and lie within the bounds of the step response

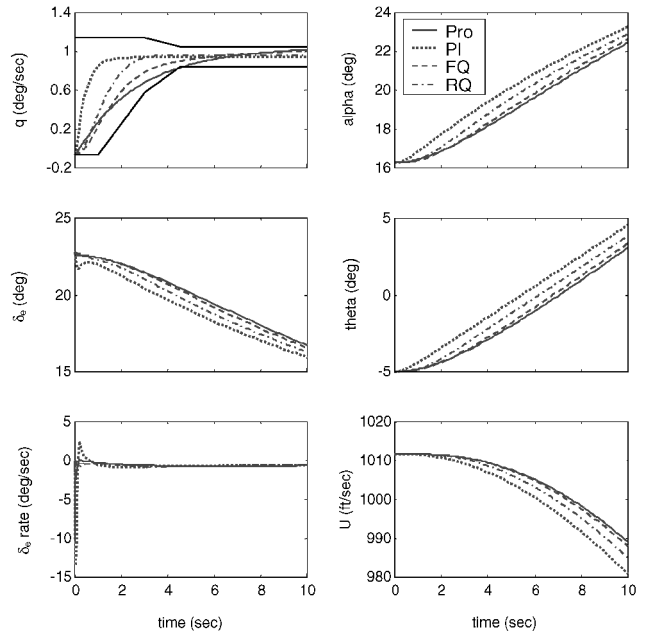


Fig. 9 Responses of closed-loop inverted pitch dynamics test cases.

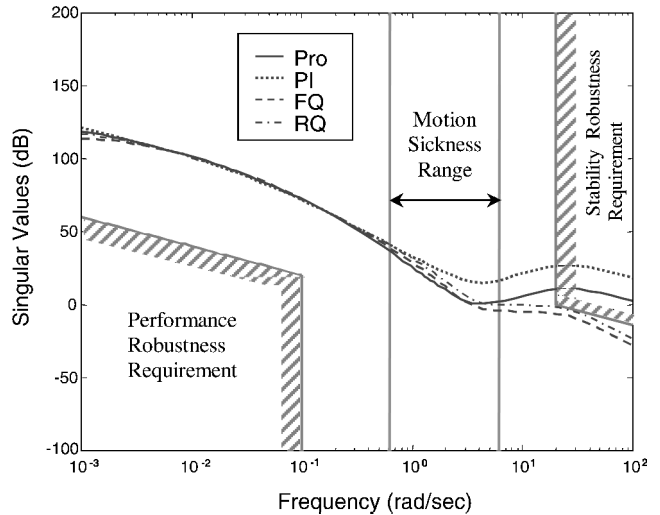


Fig. 10 Sigma-Bode plot of closed-loop inverted pitch dynamics test cases.

Table 2 Quadratic cost and passenger comfort index: pitch-rate case

Desired dynamics	Cost	Comfort index
Proportional	867.8	3.80
Proportional integral	1876.9	4.26
Flying quality	960.0	3.91
Ride quality	1271.9	4.15

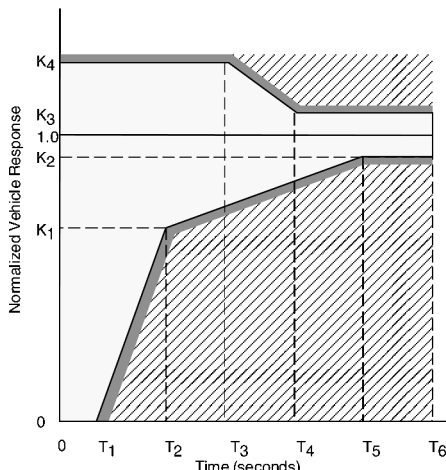


Fig. 8 Time-domain performance specifications.

Command	Amplitude			
	K1	K2	K3	K4
α to 2°	0.63	0.9	1.1	1.2
q to 1°/sec				

Command	Amplitude					
	T1	T2	T3	T4	T5	T6
α to 2°	1.0	3.0	3.0	4.5	4.5	6.0
q to 1°/sec						

Table 3 Compliance with design specifications: pitch-rate case

Desired dynamics	Step response	Control responses	Robustness constraints	Motion sickness
Proportional	✓	✓	—	—
Proportional integral	✓	✓	—	—
Flying quality	✓	✓	✓	✓
Ride quality	✓	✓	✓	✓

Table 4 Quadratic cost and passenger comfort index: angle-of-attack case

Desired dynamics	Cost	Comfort index
Proportional	130.4	2.56
Proportional integral	172.0	2.60
Flying quality	142.4	2.58
Ride quality	139.7	2.61

Table 5 Compliance with design specifications: angle-of-attack case

Desired dynamics	Step response	Control responses	Robustness constraints	Motion sickness
Proportional	✓	✓	—	—
Proportional integral	✓	✓	—	—
Flying quality	—	✓	✓	✓
Ride quality	✓	✓	✓	✓

envelope, thereby satisfying the time-domain requirements. The fast response of the proportional integral form and its correspondingly higher elevon rate is a design tradeoff between time-domain and frequency-domain requirements. The initial gains for this form and the proportional form easily satisfied the time-domain requirements, but required tuning to higher values to satisfy the high-frequency stability requirements (Fig. 10). Using gain as the only compensator, it was not possible to satisfy the high-frequency stability robustness requirement for the proportional and proportional integral forms, even with tuning. Augmenting these forms with dynamic compensation might provide the desired performance, but is beyond the scope of this study. Although the resulting set of gains that satisfies the low-frequency requirements drives the system harder than necessary to satisfy the time-domain specifications, elevon position and rate are within limits at all times. Considering the frequency range for motion sickness indicated in Fig. 10, the proportional form provides the least attenuation in this range. Although it provides more attenuation, the proportional integral form does have a positive slope in the higher end of the range, like the proportional form. The flying-quality and ride-quality forms roll off throughout the motion-sickness range, thereby providing the best motion-sickness alleviation. The quadratic cost and passenger-ride comfort index values shown in Table 2 indicate that for the same step input the proportional form and flying-quality forms had the lowest and nearly equivalent quadratic costs and produced passenger ratings corresponding to somewhat comfortable, whereas the proportional-integral and ride-quality forms by comparison had nearly double the quadratic costs and produced ride qualities corresponding to acceptable (neutral). The summary of compliance with specifications for each form of desired dynamics is summarized in Table 3 and shows that only the flying-quality and ride-quality forms satisfy all specifications. All factors considered, the ride-quality form is judged to be best overall and is used as the form to evaluate inverted pitch dynamics over a range of Mach numbers.

Results for the closed-loop inverted angle-of-attack dynamics test case are presented in Figs. 11 and 12 and Tables 4 and 5. Figure 11 shows that the flying-quality form violates both the lower and upper boundaries of the angle-of-attack envelope, whereas the other three forms satisfy the time-domain specifications. With gain as the only compensator, tuning of the flying-quality gains could not satisfy the time-domain specifications. Like the inverted pitch dynamics case, the proportional-integral form produces a rapid response with a higher initial elevon rate than the other forms, again resulting from

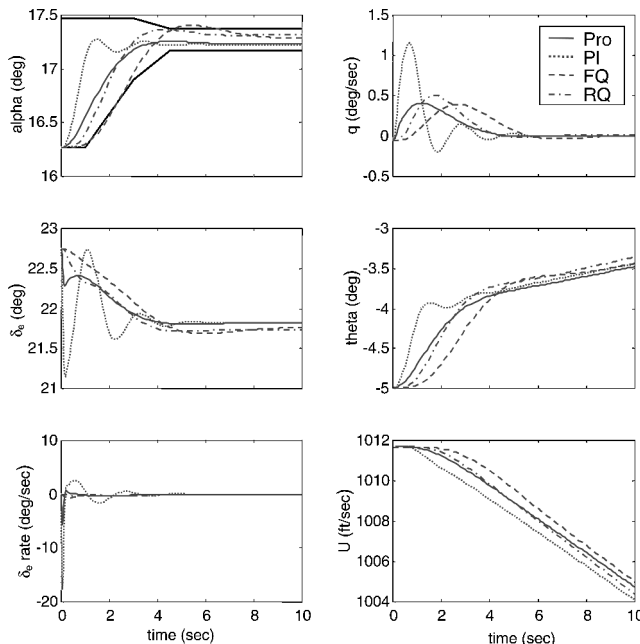


Fig. 11 Responses of closed-loop inverted angle-of-attack test cases.

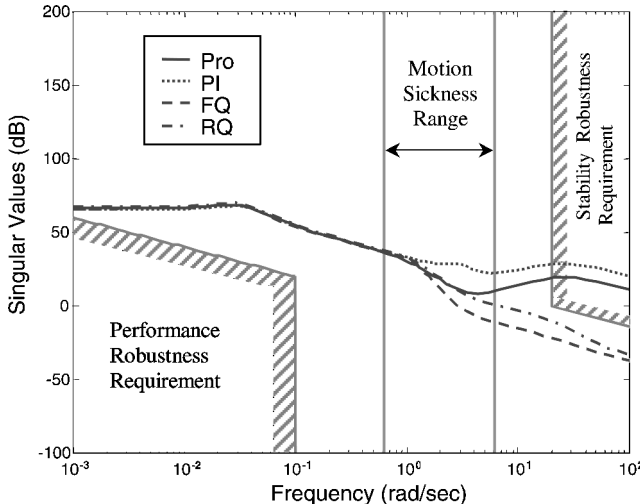


Fig. 12 Sigma-Bode plot of closed-loop inverted angle-of-attack test cases.

the gain tuning required to satisfy as best as possible the frequency-domain requirements shown in the sigma-Bode plot (Fig. 12). However, elevon position and rate limits are not exceeded. The proportional form also satisfied the time-domain specifications, but again violated the high-frequency stability robustness bound, in spite of gain tuning. Considering the frequency range for motion sickness, Fig. 12 shows that the flying-quality and ride-quality forms roll off and attenuate motion, whereas the proportional and proportional-integral forms do not. Interestingly, Table 4 shows that all four forms are very similar in terms of cost, in spite of the noncompliance of the flying-quality form and the rapid response of the proportional-integral form. Each of the forms also produce a passenger rating of comfortable. Table 5 summarizes specification compliance for each form. Only the ride-quality form satisfies all four criteria and is used as the form to evaluate inverted angle-of-attack dynamics over a range of Mach numbers.

Figures 13 and 14 illustrate the performance of pitch-rate and angle-of-attack controllers that use the ride-quality form of desired dynamics over the subsonic, transonic, and hypersonic flight conditions listed in the Appendix. The ride-quality form is used because it satisfied all specifications and requirements for both the pitch-rate and angle-of-attack controllers at the transonic flight condition. Note that the time histories in Figs. 13 and 14 represent perturbation

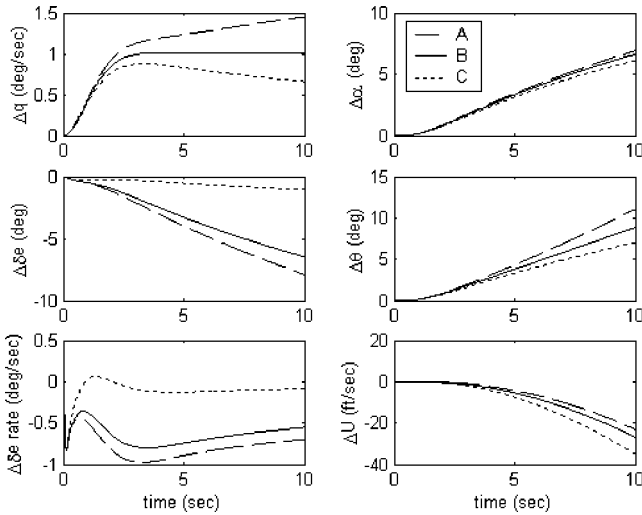


Fig. 13 Inverted pitch dynamics using ride quality at different Mach numbers.

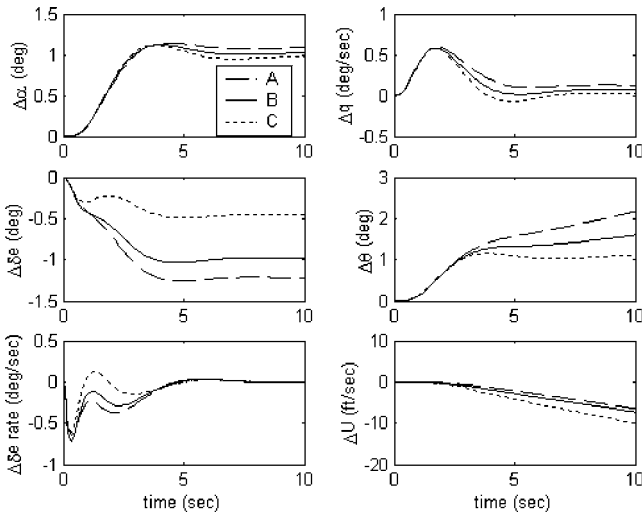


Fig. 14 Inverted angle-of-attack dynamics using ride quality at different Mach numbers.

states, not the total states as shown in Figs. 9 and 11. By plotting the perturbation states, the time histories are in essence “normalized” to facilitate comparison between these flight regimes and trim conditions. Figure 13 shows that although each pitch-rate response is similar the hypersonic flight condition C violates the response envelope. Figure 14 exhibits bounded and well-behaved angle-of-attack responses that are nearly identical in magnitude and behavior. Overall, these results would indicate that the ride-quality form is a suitable candidate form of desired dynamics for the type and application of dynamic-inversion controllers investigated in this paper, as it produces stable, bounded responses across different flight regimes.

Conclusions

Four candidate forms of desired dynamics were used to design pitch-rate and angle-of-attack dynamic inversion controllers using linearized models of a generic X-38 type reentry vehicle at subsonic, transonic, and hypersonic flight conditions. Time-domain specifications and robustness requirements, formulated as frequency-dependent bounds on singular values, were used with a quadratic cost function and a passenger-ride comfort index to evaluate the closed-loop performance of each candidate form. For the particular candidate forms, specifications, requirements, and evaluation criteria investigated in this paper, the following conclusions are drawn:

1) In terms of quadratic cost and passenger-ride comfort index, the impact of the form of desired dynamics on closed-loop system performance depends upon the type of dynamic inversion being used,

for example, a single dynamic-inversion loop or a two-timescale approach with two loops. The two-loop inversion (angle-of-attack controller) was essentially insensitive to the form of desired dynamics used, whereas the single-loop inversion (pitch-rate controller) was strongly sensitive, with the proportional and flying-quality forms producing the best performance in terms of these metrics.

2) Certain candidate forms incur significant design tradeoffs between robustness and time-domain performance. For example, gain tuning the proportional-integral form to satisfy low-frequency performance robustness requirements resulted in larger gains, which produced aggressive responses. Although the responses remain within time-domain specifications, they produced larger than desired accelerations and rates, which result in higher values of quadratic cost and a less satisfactory ride comfort level. This was particularly seen for the pitch-rate controller.

3) For both controllers all four candidate forms could be tuned to satisfy the low-frequency performance robustness requirements, but the proportional and proportional-integral forms could not be tuned to satisfy the high-frequency stability robustness requirements, using gain compensation only. The flying-quality form was the only one whose gains could not be tuned to satisfy the time-domain specifications of both controllers.

4) All four candidate forms produced equivalent levels of passenger-ride comfort for the angle-of-attack controller, but the proportional and flying-quality forms were best in terms of ride comfort for the pitch-rate controller. Additionally, for both controllers motion-sickness alleviation was achieved by the flying-quality and ride-quality forms, but not for the proportional and proportional-integral forms, particularly in the high-frequency band of the motion-sickness range.

5) The ride-quality form was the only one that satisfied all specifications and evaluation criteria for both controllers at the transonic flight condition. When evaluated for both controllers over a range of subsonic, transonic, and hypersonic flight conditions, the responses were within specifications for the angle-of-attack controller, but not for the pitch-rate controller. All specifications and factors considered, ride-quality dynamics for a two-loop angle-of-attack inversion controller provided the best overall performance.

Appendix: Generic X-38 Linear Models

State-space parametric linear model of longitudinal dynamics, as fully defined in Ref. 25:

$$\begin{bmatrix} \dot{u} \\ \dot{\alpha} \\ \dot{q} \\ \dot{\theta} \end{bmatrix} = \begin{bmatrix} X_u & X_\alpha & 0 & -g \\ \frac{Z_u}{u_o} & \frac{Z_\alpha}{u_o} & 1 + \frac{Z_q}{u_o} & 0 \\ M_u + M_\alpha \frac{Z_u}{u_o} & M_\alpha + M_\alpha \frac{Z_\alpha}{u_o} & M_q + M_\alpha & 0 \\ 0 & 0 & 1 & 0 \end{bmatrix} \begin{bmatrix} u \\ \alpha \\ q \\ \theta \end{bmatrix} + \begin{bmatrix} X_{\delta_e} \\ \frac{Z_{\delta_e}}{u_o} \\ M_{\delta_e} + M_\alpha \frac{Z_{\delta_e}}{u_o} \\ 0 \end{bmatrix} \delta_e$$

State-space nonparametric linear models of longitudinal (all angular quantities are in radians) dynamics:

Flight condition A (subsonic; Mach 0.63; 20,310 ft):

$$A_1 = \begin{bmatrix} -0.036 & -4.14 & 0 & -32.17 \\ 0 & -0.18 & 1 & 0 \\ 0 & -2.55 & -0.23 & 0 \\ 0 & 0 & 1 & 0 \end{bmatrix}, \quad B_1 = \begin{bmatrix} -4.19 \\ -0.04 \\ -2.28 \\ 0 \end{bmatrix}$$

Flight condition B (transonic; Mach 1.04; 46,379 ft):

$$A_1 = \begin{bmatrix} -0.0335 & -22.5 & 0 & -32.2 \\ 0 & -0.0944 & 1.0 & 0 \\ 0 & -1.94 & -0.188 & 0 \\ 0 & 0 & 1 & 0 \end{bmatrix}$$

$$B_1 = \begin{bmatrix} -8.83 \\ -0.0196 \\ -2.02 \\ 0 \end{bmatrix}$$

Flight condition C (hypersonic; Mach 4.11; 101,843 ft):

$$A_1 = \begin{bmatrix} -0.0093 & -41.13 & 0 & -32.17 \\ 0 & -0.018 & 1 & 0 \\ 0 & -1.08 & -0.015 & 0 \\ 0 & 0 & 1 & 0 \end{bmatrix}$$

$$B_1 = \begin{bmatrix} -6.95 \\ -0.0029 \\ -2.28 \\ 0 \end{bmatrix}$$

Acknowledgments

This research is supported by the NASA Johnson Space Center, under Grant NAG 9-1085. The technical monitor is Mark M. Hammerschmidt. This support is gratefully acknowledged by the authors. The authors also thank the Associate Editor and reviewers for their many insightful comments and suggestions, which improved the paper.

References

¹Dorf, Richard, C., and Bishop, Robert, H., *Modern Control Systems*, 9th ed., Prentice-Hall, Upper Saddle River, NJ, 2001, pp. 553-630.

²Stevens, B., and Lewis, F., *Aircraft Control and Simulation*, Wiley, New York, 1992, pp. 236-331.

³Colgren, R., and Enns, D., "Dynamic Inversion Applied to the F-117A," *Proceedings of the AIAA Modeling and Simulation Technologies Conference*, AIAA, Reston, VA, 1997, pp. 275-284.

⁴Enns, D., Bugajski, D., Hendrick, R., and Stein, G., "Dynamic Inversion: An Evolving Methodology for Flight Control Design," *International Journal of Control*, Vol. 59, No. 1, 1994, pp. 71-91.

⁵Adams, R. J., Buffington, J. M., and Banda, S. V., "Design of Nonlinear Control Laws for High-Angle-of-Attack Flight," *Journal of Guidance, Control, and Dynamics*, Vol. 17, No. 4, 1994, pp. 737-746.

⁶Adams, R. J., and Banda, S. V., "Robust Flight Control Design Using Dynamics Inversion and Structured Singular Value Synthesis," *IEEE Transactions on Control Systems Technology*, Vol. 1, No. 2, 1993, pp. 80-92.

⁷Durham, W. C., "Dynamic Inversion and Model-Following Control," *Proceedings of the AIAA Guidance, Navigation, and Control Conference*, AIAA, Reston, VA, 1996, pp. 1-12.

⁸Smith, P., and Berry, A., "Flight Test Experience of a Non-Linear Dynamic Inversion Control Law on the VAAC Harrier," AIAA Paper 2000-3914, Aug. 2000.

⁹Ostroff, A. J., and Bacon, B. J., "Force and Moment Approach for Achievable Dynamics Using Nonlinear Dynamic Inversion," *Proceedings of the AIAA Guidance, Navigation, and Control Conference and Exhibit*, AIAA, Reston, VA, 1999, pp. 424-434.

¹⁰Brinker, J. S., and Wise, K. A., "Stability and Flying Qualities Robustness of a Dynamic Inversion Aircraft Control Law," *Journal of Guidance, Control, and Dynamics*, Vol. 19, No. 6, 1996, pp. 1270-1277.

¹¹Honeywell Technology Center, Lockheed Martin Skunk Works, and Lockheed Martin Tactical Aircraft Systems, "Application of Multivariable Control Theory to Aircraft Control Laws: Final Report: Multivariable Control Design Guidelines, Flight Dynamics Directorate," Wright Lab., WL-TR-96-3099, Wright-Patterson AFB, OH, May 1996.

¹²Fer, H., and Enns, D. F., "An Approach to Select Desired Dynamics Gains for Dynamic Inversion Control Laws," *Proceedings of the AIAA Guidance, Navigation, and Control Conference*, AIAA, Reston, VA, 1997, pp. 755-769.

¹³Reiner, J., Balas, G. J., and Garrard, W. L., "Robust Dynamic Inversion for Control of Highly Maneuverable Aircraft," *Journal of Guidance, Control and Dynamics*, Vol. 18, No. 1, 1995, pp. 18-24.

¹⁴Snell, S. A., and Stout, P. W., "Robust Longitudinal Control Design Using Dynamic Inversion and Quantitative Feedback Theory," *Journal of Guidance, Control, and Dynamics*, Vol. 20, No. 5, 1997, pp. 933-940.

¹⁵Georgie, Jennifer, "Selection of Desired Dynamics for Dynamic Inversion Controlled Re-Entry Vehicles," M.S. Thesis, Aerospace Engineering Dept., Texas A&M Univ., College Station, TX, Aug. 2001, pp. 13-16.

¹⁶Snell, S. A., "Preliminary Assessment of the Robustness of Dynamic Inversion Based Flight Control Laws," *Proceedings of the AIAA Guidance, Navigation and Control Conference*, AIAA, Washington, DC, 1992, pp. 206-216.

¹⁷"Military Standard Flying Qualities of Piloted Aircraft," Mil-STD-1797A, Jan. 1990.

¹⁸Kautsky, J., Nichols, N. K., and Van Dooren, P., "Robust Pole Assignment in Linear State Feedback," *International Journal of Control*, Vol. 41, No. 5, 1985, pp. 1129-1155.

¹⁹Junkins, J. L., and Kim, Y., *Introduction to Dynamics and Control of Flexible Structures*, AIAA, Washington, DC, 1993, pp. 256-259.

²⁰"Shuttle Engineering Simulator X-38 V201 Actuator File," NASA, Johnson Space Center, Internal Memo, Clear Lake, TX, Oct. 1998.

²¹Richards, L. G., Kuhlthau, A. R., and Jacobson, I. D., "Passenger Ride Quality from Commercial Airline Flights," NASA TM X-3295, Aug. 1975, pp. 409-436.

²²Duncan, N. C., and Conley, H. W., "Demographic and Psychological Variables Affecting Test Subject Evaluations of Ride Quality," NASA TM-X-3295, Nov. 1975, pp. 287-321.

²³Ito, D., and Valasek, J., "Robust Dynamic Inversion Controller Design and Analysis to the X-38 Vehicle," AIAA Paper 2001-4380, Aug. 2001.

²⁴Suikat, R., Donaldson, K., and Downing, D., "Analysis of a Candidate Control Algorithm for a Ride-Quality Augmentation System," *Journal of Guidance, Control, and Dynamics*, Vol. 12, No. 4, 1989, pp. 505-513.

²⁵Nelson, Robert, C., *Flight Stability and Automatic Control*, 2nd ed., McGraw-Hill, New York, 1989, pp. 78-81.